IEEE J Electromagn RF Microw Med Biol. 2022 Aug 17;6(4):477–484. doi: 10.1109/JERM.2022.3194727

Combating Coronavirus Using Resonant Electromagnetic Irradiation

Khalil H Sayidmarie [1], Beadaa Mohammed [2,✉], Asmaa J Mohammed [3], Amin Abbosh [2]

Author information Article notes Copyright and License information

PMCID: PMC9728540 PMID: 36514675

Abstract

The interaction of electromagnetic (EM) waves with the COVID-19 virus is studied to define the frequencies that cause maximum energy absorption by the virus and the power level needed to cause a lethal temperature rise. The full-wave EM simulator is used to model the virus and study the effects of its size and dielectric properties on the absorbed power across a wide range of frequencies. The results confirm potential resonance conditions, where specific frequencies produce maximum absorption and subsequent temperature rise that can destroy the virus. Furthermore, the study confirms that maximum power deposition in the virus occurs at specific wavelengths depending on its size. Also, the simulation is used to find the power required to destroy the virus and determine the total power required to destroy it in an oral activity, such as coughing, made by infected individuals. Furthermore, the study explained why irradiation by UV-C band is effective to decrease virus activity or even eradicate it.

Keywords: Electromagnetic waves, Coronavirus, COVID-19, nanoparticles, electromagnetic absorption

I. Introduction

In Late 2019, an epidemic identified as the novel coronavirus (COVID-19) caused a sudden increase in hospitalizations [1]. The virus rapidly spread across the globe [2]–[6], and thus the World Health Organization (WHO) announced it a global pandemic [6], [7]. COVID-19 is a new member of the beta-coronavirus family related to the known severe acute respiratory syndrome coronavirus (SARS-CoV) [8], [9]. However, COVID-19 is more transmittable between humans [8], [9]. The virus still causes many deaths around the world. Luckily, there have been enormous progress and successes in developing various vaccines. To prevent the spread of the virus, the World Health Organization (WHO) has issued many devices, such as social distancing, wearing a face mask, and handwashing. It was advised that applying soap long enough can disrupt and break down the outer layer (i.e., envelop), making the virus no longer functioning [10]–[14]. In addition, scientists working in different fields have been trying to understand the virus's behavior to develop the required vaccines and treatments.

On another line, the scientific community has been adapting its existing skills in developing and improving technologies that can fight COVID-19. In that regard, ultraviolet (UV) electromagnetic (EM) waves have been recommended as a tool to reduce the daily growth rate or kill the virus by using high doses of UV to disinfect equipment and buildings while using safe levels of UV doses [15]–[18]. In addition, the interaction between EM waves and the virus has been investigated [19]. The previously mentioned research has concluded that more research is required to find EM-based tools or methods to prevent the virus from spreading. These studies were based on experimental tests, with no explanation of the physical principles regarding why a particular band of frequencies influences the virus more than others or whether other bands could be more effective.

When EM waves illuminate a small biological object, such as the virus body, an EM field is induced in the internal body. The subsequent power absorption by the virus results in a specific resonance behavior [19], [20]. That internal field is absorbed by the object's dielectric material, increasing the biological material's temperature. Increasing the temperature to exceed the thermal thresholds of the biological material cell can kill that cell. The internal EM field distribution, absorption characteristics, and the scattered EM waves of any object, including the virus body, depend on the used frequency, object's geometry, polarization of the incident wave, and physiological parameters (i.e., frequency-dependent dielectric properties of the biological material). Hence, it is essential to understand how EM waves and their wavelength, virus size, and shape can affect absorption to find the optimal interaction regime and wavelength that cause the maximum absorption inside the virus body. This investigation will enable the development of devices or techniques that can thermally damage, disintegrate, or neutralize the COVID-19 body. Since the virus body consists of

biological materials, a specific resonance is expected to significantly increase the absorbed EM energy when the incident wavelength is comparable to the virus body. The virus body might be destroyed at the resonant frequencies due to the high level of absorbed energy from overexposure [15], [19], [20].

This paper uses CST Microwave Studio simulation [21] to study the interaction between EM waves and the COVID-19 virus in the frequency band of 100-6000 THz. A realistic virus model, which includes its RNA, envelop layer, and spikes, is utilized in this investigation. In addition, the total power loss in each tissue type is calculated, and the effect of the virus size on the total loss in the virus body is also investigated to explain the specific frequency bands, or wavelengths, that can be used to destroy COVID-19. The paper is organized as follows; after an introductory section, the methods are discussed in Section II. Section III presents the obtained simulation results and discussion, while the conclusions are listed in Section IV.

II. Virus Model and Simulation Setup

A. Virus Model

The COVID-19 genome structure is a pleomorphic or spherical single-stranded ribonucleic acid (RNA), protein-like biological material representing the virus's internal structure [22], [23]. A membrane encloses the RNA covered by spikes made of a protein-like biological material protruding from the surface, enabling the virion's attachment to the host's cell membrane [22]–[28]. The membrane layer surrounding most viruses such as influenza and herpes simplex is called a “lipid envelop”. Thus, the membrane layer is similar to the fat biological material. Also, the RNA and spikes of COVID 19 are mainly protein [22]–[29], and thus they are closer to the dielectric properties of the muscle tissue, which is mainly protein consistent. The ultrastructural morphology exhibited by COVID-19 created at the Centers for Disease Control and Prevention (CDC), showing the spikes that adorn the virus's outer surface microscopically, is shown in Fig. 1. The average diameter of the virus varies from 50 to 200 nm [22], [23] as concluded from Table I. Some studies used electron microscope images to find number of viruses in a given volume [25], [28]. As with other biological objects, one should expect the virus and its variants to have a specific range of sizes. Therefore, looking at Table I, an average size of 100 nm was assumed in this work. The results of smaller and larger are also presented for comparison [22].

Fig. 1.

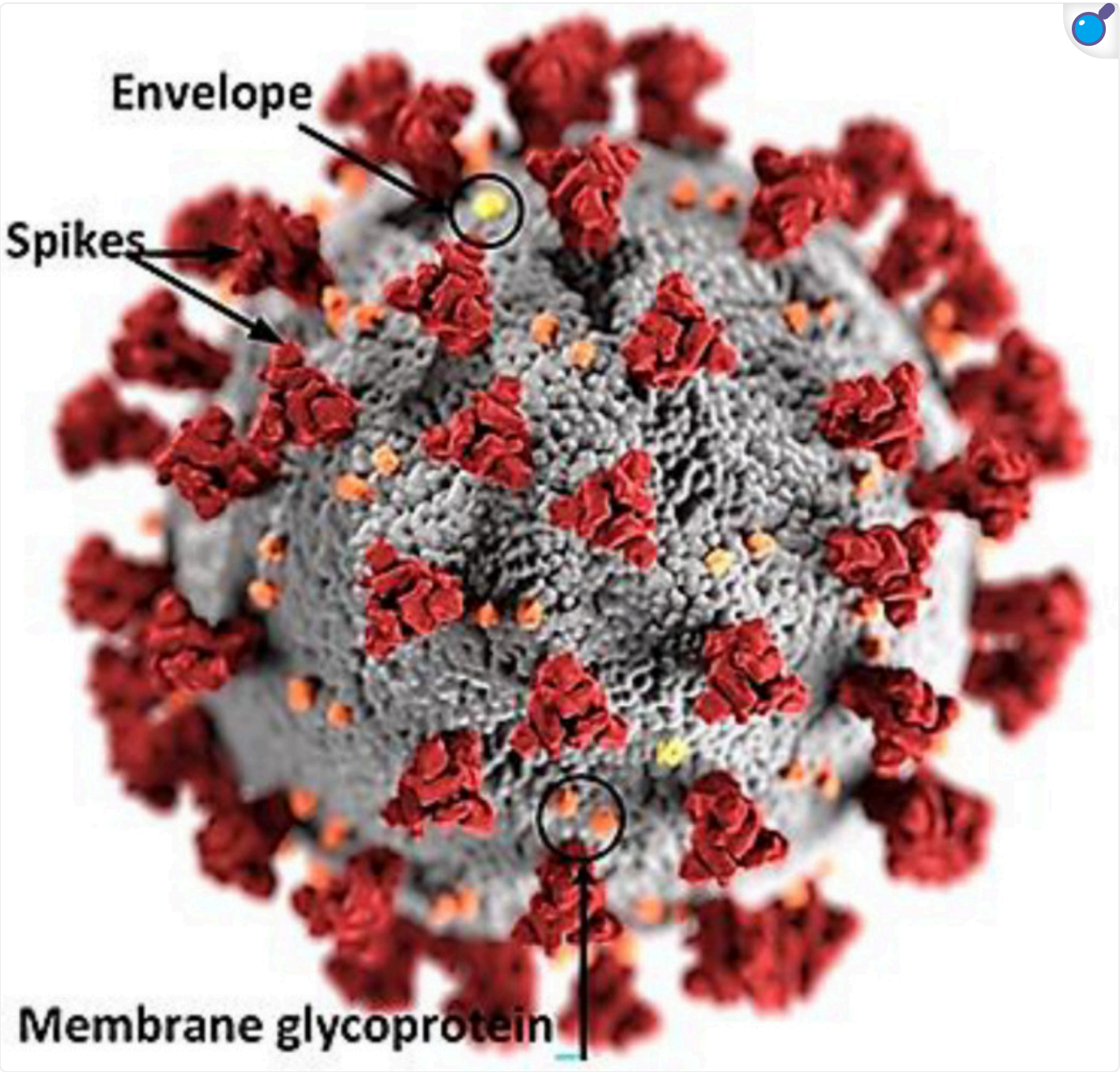

Open in a new tab

The outer look of COVID-19 under microscopically viewed at the Centers for Disease Control and Prevention (CDC) [23].

TABLE I. List of Some Former Studies That Reported the Average Diameter of covid-19 in Nanometer (nm).

Ref.	Diameter	Average diameter	Spikes length	Notes:
	(nm)		(nm)	
[1]	60-140	100	9-12	Based on SAR-Cov-2
[2]	120-160	140	20	Used diam = 140 nm Spike length = 20nm in the simulation
[5]	50-200	125		
[15]	30-100	65		
[18]	80-120	100		
[20]	100-150	125	NA	
[21]	60-140	100	9-12	From Transmission Electron Microscopy
[22]	80-120	100		
[23]	60-140	100		
[25]	60-140	100	9-12	Referred to [21]

Open in a new tab

The documented studies in the literature, such as [30]–[35] indicated that the known mutations so far mainly cause changes in the sequence of RNA protein, in addition to other possible changes to spikes number and protein type. We concluded based on known details at this stage that mutations may not significantly change the dielectric properties of the virus envelope, which is the most critical factor in the investigated resonance frequency method. Nevertheless, since there is no consensus in the literature on the exact size of the virus, or the virus might take different sizes due to unknown reasons, this study also investigates the effect of resonance irradiation with different

virus size. If any future mutation is confirmed to cause a significant change to the structure and dielectric properties of the virus (RNA, spikes, and the envelope), a further study is needed.

B. Simulation Setup

The simulation is performed on the expected or reported range of virus size to help understand the interaction of the EM waves with the electrical properties of the virus body parts (i.e., spikes, RNA, and envelope). This section investigates the effect of the virus size on the resonant frequency for various sphere (i.e., RNA) diameters, 50 nm, 100 nm, 150 nm, and 200 nm, representing the possible size range COVID-19. First, the enveloping layer is modeled as a 2 nm layer surrounding the RNA sphere. Next, the spikes are added to the structure to create a realistic virus body. Each of these spikes is modeled as a cone structure (0.5 nm base diameter, 2 nm top diameter, and 10 nm height) created from the outer layer (i.e., the virus envelope) [25], [26]. As this model has used two types of material (fat and protein) and three shapes (sphere, shell, and spikes), then it can be considered more realistic compared to other models like the one in [19], which used a sphere and a thin shell representing the spikes. Finally, the simulation determines the resonant frequency, which causes maximum absorption.

A wide frequency range of 100-6000 THz is used to assess the response of the virus model and find the frequencies at which there is maximum power deposition in the virus that can deactivate the virus of different sizes and destroy its ability to multiply and cause disease. The chosen frequency band in this investigation covers the infrared, visible, and higher UV in the nanometer-wavelength, which were shown to be germicidal [17], [36]–[41] as the nucleic acids of the germs strongly absorb these wavelengths. Therefore, there should be optimum wavelengths that lead to maximum power deposition in the virus body, cause damage to its nucleic acid and prevent replication, resulting in the organism's death or inactivation. The wavelengths that result in maximum power deposition will be recommended for combating the virus

In the simulation, power loss and power flow monitors were used to estimate the power loss in the virus body and find the resonant frequency when the EM wave interacts with it across the frequency band of 100-6000 THz. A uniform plane wave of the unit intensity of electric-field value in ($Volt/m$) with linear polarization is used as a source of the EM field to irradiate the virus body (Fig. 2). Also, a circular polarization was applied to check its effect on the virus body structure. The dielectric properties of the virus body define the distribution of the EM field inside the virus. Therefore, accurate modelling of the dielectric properties of the virus's biological materials is required to estimate EM fields accurately and thus absorption inside the virus body.

Fig. 2.

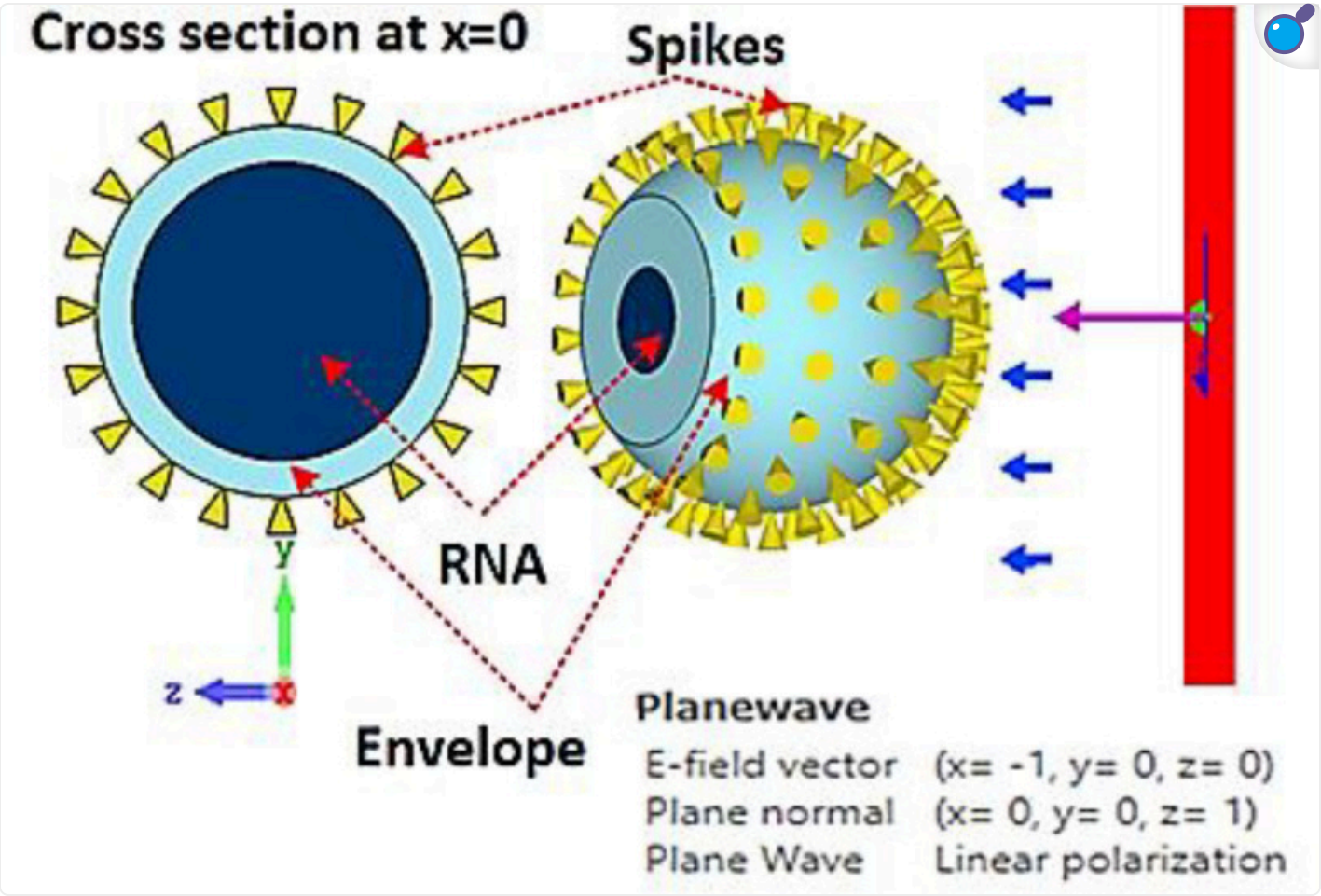

Open in a new tab

Simulation setup of realistic COVID-19 virus structure.

Although there is no specific data about the RNA, envelops, and spikes dielectric properties primarily in the investigated frequency band, the information provided in [42] is used as a guide to find out the nearest dielectric properties from the most common source of dielectric properties of biological tissues [43]. The fat or lipid-like biological material's dielectric properties represent the membrane layer (i.e., the outer envelope fatty layer). On the other hand, the dielectric properties of the RNA and the spikes are emulated using the dielectric properties of biological muscle material. The RNA and spikes are protein-consistent materials [22], [27]–[29], [44], which are thus like the muscle tissue, which is considered the main source of protein (i.e., it contains more than 80% protein) [45]. Therefore, to simulate the realistic dielectric properties of the virus, the relevant

dielectric properties of biological materials available in [43] were used. The simulation setup of the realistic COVID-19 virus structure is shown in Fig. 2.

The absorbed power can define the interaction of EM waves with a macroscopic biological object depending on its permittivity and conductivity, knowing that the permeability of biological materials is constant and equal to that of a vacuum. The dielectric properties of biological materials are frequency-dependent and can be described by the relative complex dielectric properties (ε^*) that is expressed as:

$$\varepsilon\ (\omega) = \varepsilon'\ (\omega) - j\varepsilon''\ (\omega) = \varepsilon_r\ - j\frac{\sigma}{\omega\varepsilon_0}$$

$$\ldots,\ldots,\ldots,\ldots \quad (1)$$

where $\varepsilon'(\omega)$ is the real part and represents the relative permittivity of the dielectric constant (ε_r), while $\varepsilon''(\omega)$ is the imaginary part and can be used to estimate the dielectric loss factor and conductivity (σ) in Sm^{-1}, $\varepsilon_0(Fm^{-1})$ is the permittivity free space, and ω is the angular frequency used to define frequency-dependent properties of the dielectric material.

In the simulation, a superposition of the first and second-order Debye model is used to obtain the relaxation process of the biological materials expressed as [44]:

$$\varepsilon\ (\omega) = \varepsilon_\infty\ + \frac{(\varepsilon_s - \varepsilon_\infty)}{1 + j\omega\tau} \ldots\ldots\ldots\ldots \quad (2)$$

where $\varepsilon_\infty, \varepsilon_s$ are the dielectric constant at high and low frequency, respectively, and τ is the time constant, also called the relaxation time, which determines the frequency range of significant changes. The recommended data for the dielectric properties (i.e., the relative permittivity and conductivity) of COVID-19 biological materials are then used in the simulator [42]. Fig. 3 shows the variation of the relative permittivity and conductivity of the constituents of the COVID-19 model across the 100-6000 THz frequency range. The relative permittivity has a slight variation with frequency. However, the conductivity has a considerable variation across the investigated frequency range.

Fig. 3.

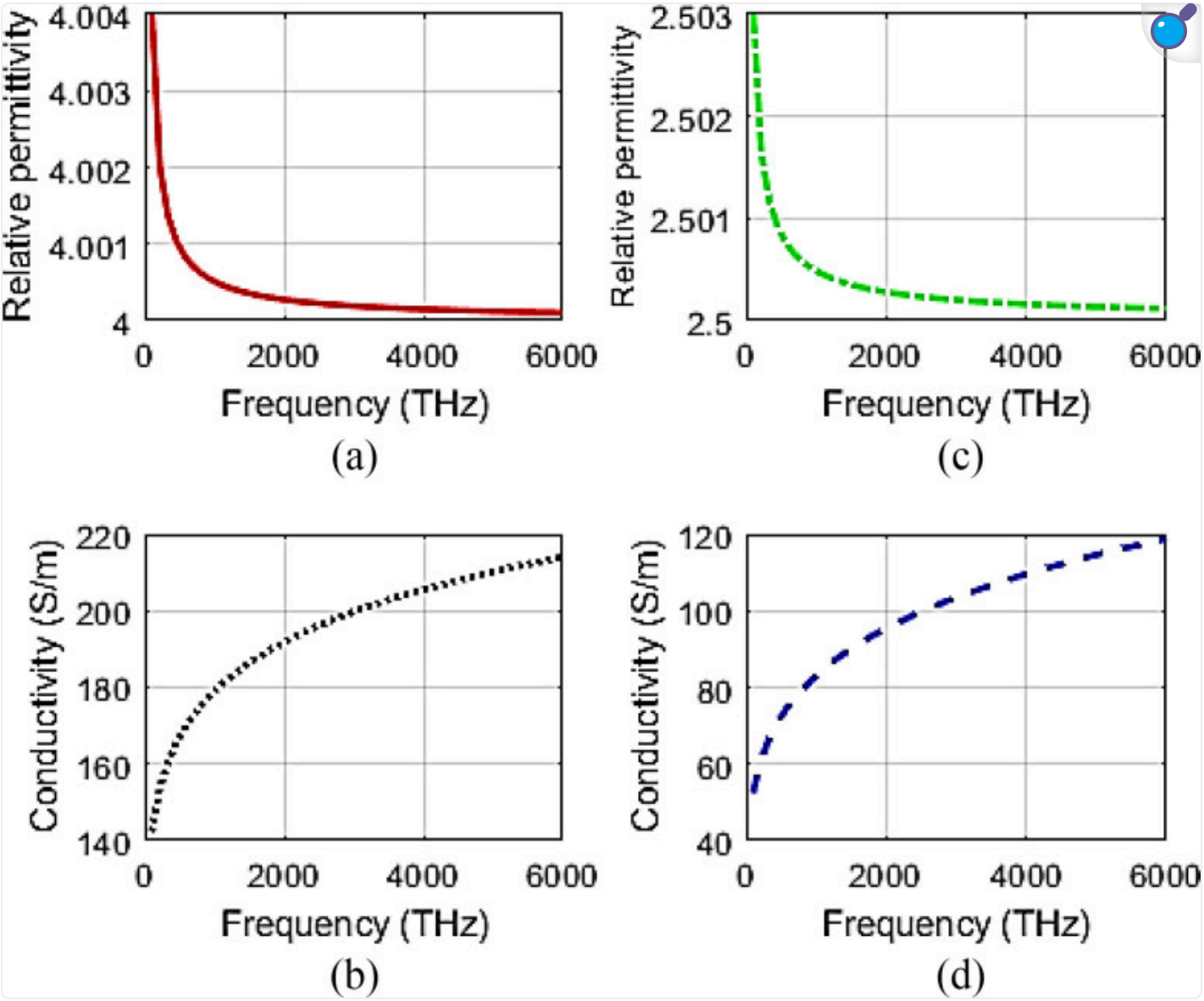

Open in a new tab

Dielectric properties of COVID-19 biological materials for the: (a), (b) RNA, and spikes, (c), (d) envelop.

The resonant behavior of the biological materials in any living tissue can be described by the Lorentz model [45]:

$$\varepsilon\ (\omega) = \varepsilon_\infty\ + \frac{(\varepsilon_s - \varepsilon_\infty)\,\omega_0^2}{\omega_0^2 + i\omega\delta - \omega^2} \ldots\ldots\ldots\ldots \quad (3)$$

Fig. 4 shows the visualization of dielectric properties for (2) and (3). The resonance is characterized by a peak in the imaginary part and a zero, or close to zero, in the real part. In the simulation, the power absorption by the frequency-dependent dielectric material of the virus body is investigated. To that end, power loss density at each frequency step was assigned across the whole frequency band. The effects of virus size on the maximum power absorbed, absorption coefficient, relative absorption cross-section and resonant frequencies are assessed.

Fig. 4.

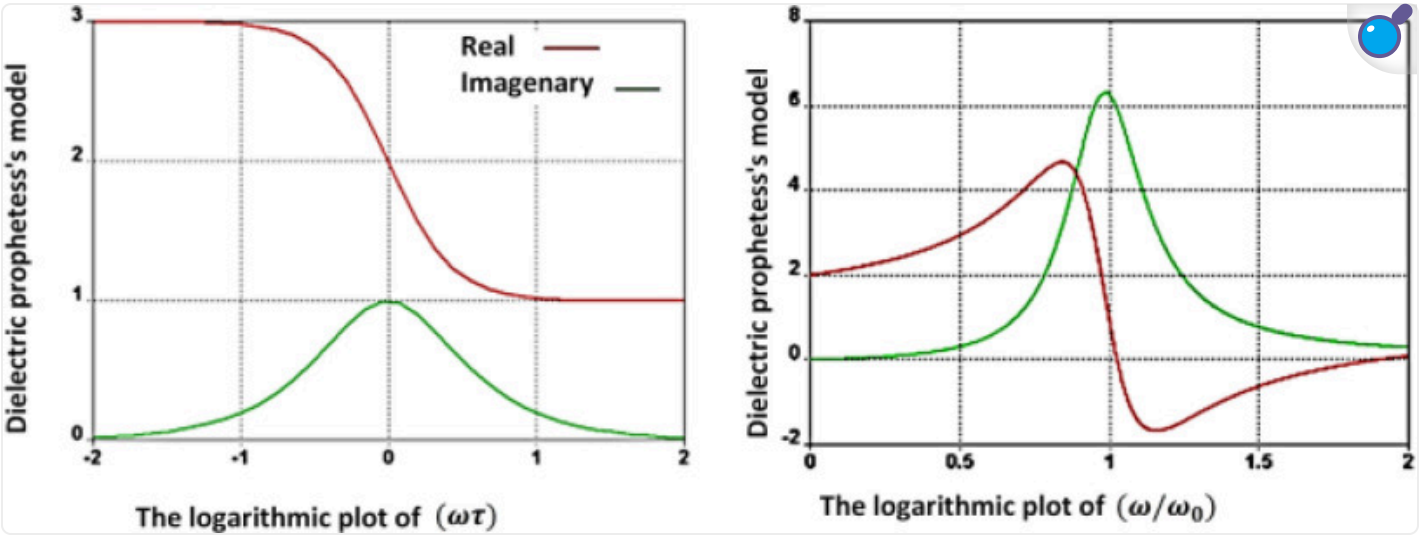

Open in a new tab

CST microwave studio representations of the dielectric properties (real and imaginary parts); (a) Debye first-order dispersion model with the relaxation process; and (b) Lorentz model with the resonance process.

According to [10]–[14], using soap long enough damages the envelope, stopping the virus functionality. Therefore, an investigation via simulation is performed to determine the required EM wave power to destroy the virus envelope. A power flow monitor was assigned with a 100 THz

step across the 100-6000 THz frequency band. The monitors were used to measure the power of the EM wave inside the virus envelope. In the simulation, the virus is modeled at the center of (x,y,z) coordinates (Fig. 2). For convenience, the EM wave sources are applied in the negative z-direction. At each frequency step, the power loss monitors provide the power reading of the EM wave transmitted from the source to the virus body. The power loss monitors calculate the power density $\left(w/cm^3\right)$ at each frequency step in the simulation environment, including the virus body and surroundings. The power lost inside the envelop layer is determined across the volume of the virus envelop layer at each selected size and estimating the required power for a single virus.

COVID-19 can be separated in many modes, mainly through aerosols (droplets). The size and quantity of the virus depend on the droplet's size and number resulting from any individual's oral activities. Those activities include coughing, sneezing, or talk droplets that contain virus particles. For example, when an infected person coughs, sneezes, or talks, aerosols (droplets) or tiny particles are spared into the air. The droplets are a liquid-biased material with different droplet sizes, containing viruses of different sizes. Therefore, the infection happens in any recipient's breath air containing the virus particles in sufficient quantity [46]–[48]. There are no exact measurements of droplets produced by oral activities such as coughing, sneezing, breathing, and phonation [49]. However, studies showed that coughing and sneezing activities particles could release about 3000 -40000 droplets [50]. Different size droplets in any of these activities may vary between 6-12 μm [49], [50]. Also, number of viruses in each droplet is different; therefore, number of viruses will differ depending on the virus and droplet sizes.

Surface transmission mode may also occur indirectly by touching surfaces such as plastic and stainless steel contaminated with virus from a cough or sneezing from an infected person, followed by touching the mouth, nose, or eyes. The virus can live for 2-3 days on those surfaces.

In addition, a common way of transmission is the airborne mode, as the virus particles can stay alive in the air for up to three hours [51]; any recipient's breathing that air leads to their infection [47]–[52]. After the oral activities, the liquid material starts to evaporate immediately, leaving the virus body in the air or on surfaces as it can stay longer. Therefore, the virus body is simulated in the air (i.e., the airborne transmitting mode of the virus is considered), and the power deposition inside a single virus body is calculated using (3). In the case of COVID-19, the RNA copies number in the oral fluid vary from an average of 7×10^6 to a maximum of 2.35×10^9 copies per millilitre [52]. The total power (P_{total}) required to destroy the viruses resulting from an oral activity containing virus copies (N_{co}) can be calculated as follows:

$$P_{total} = P_d \times N_{co} \ldots, \ldots, \ldots \quad (4)$$

Where P_d is the power required to destroy one virus.

III. Results and Discussion

A. The Resonant Absorption

The resonance absorption property results in the virus envelop for various virus sizes (Fig. 5). The variation of the total power loss with frequency in the virus envelop dielectric material shows multiple peaks of the power loss, indicating resonance at various modes. The intensity of absorption increases as the diameter of the virus increases. Moreover, the positions of the peaks shift to lower frequencies as the diameter of the RNA dielectric sphere increases, indicating, as expected, a reverse relation between the sphere's diameter and the resonant frequency. The response shows multi resonances for each of the investigated sizes of the virus. This finding agrees with the results [53] for the interaction of the incident EM wave on a dielectric sphere. Also, many resonating modes resulted in the realistic structure having multiple layers and spikes of different dielectric properties.

Fig. 5.

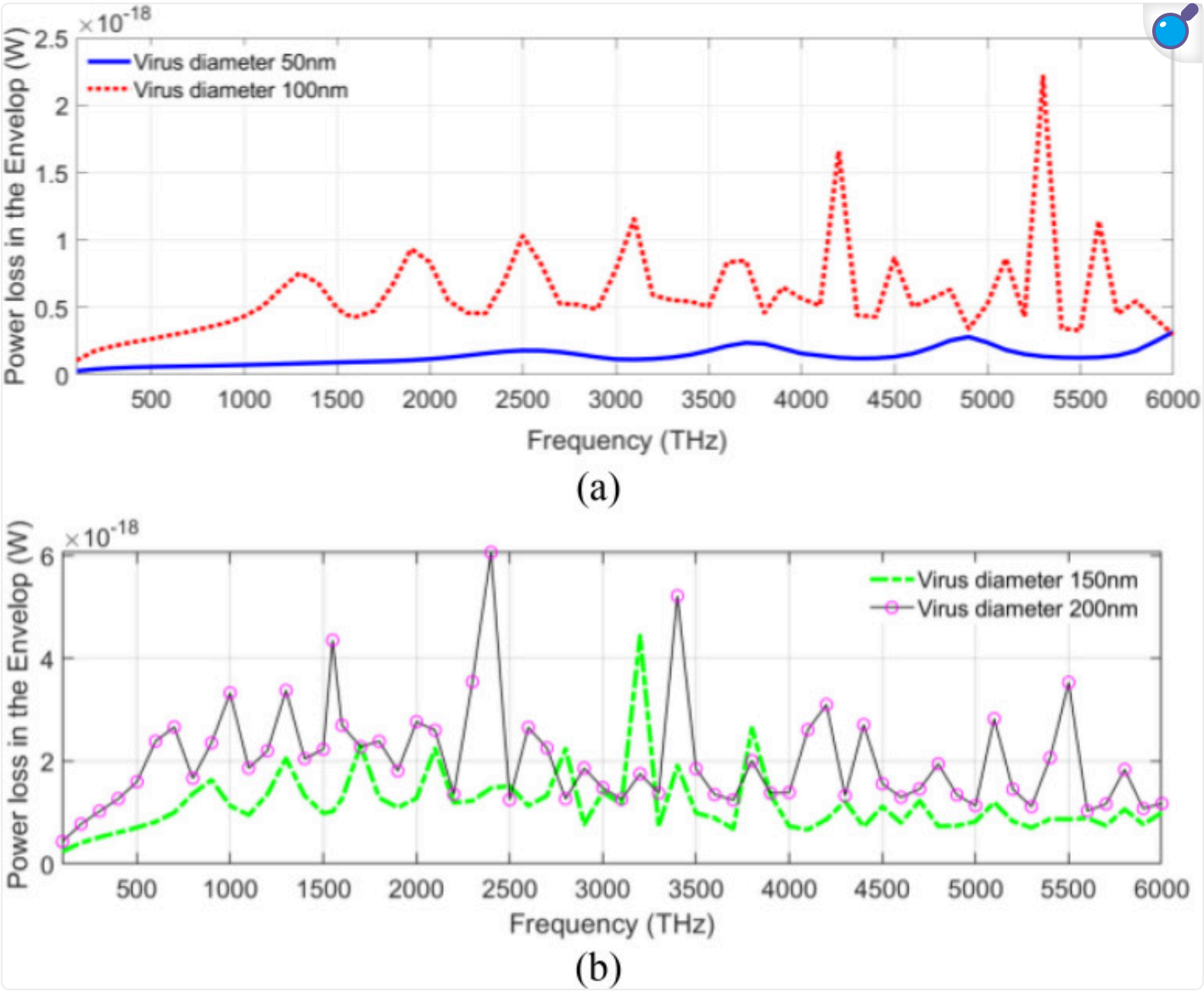

Open in a new tab

The total power loss in the virus envelops when the virus RNA diameter is (a) 50 nm and 100 nm, (b) 150 nm and 200 nm.

The virus body has a lower permittivity of $\varepsilon_r = 2.5$ for the enveloping layer and a higher value of $\varepsilon_r = 4$ for the spikes and RNA. A more considerable difference in permittivity leads to a lower effective wavelength or higher resonant frequency. In addition, more resonant frequencies result from the virus model of a larger sphere diameter. Fig. 5(b) shows more resonant frequencies

as a larger diameter of the sphere results in more degrees of freedom for the occurrence of resonances. The three lowest resonance frequencies with a virus diameter of 50 nm (see Fig. 5(a)) occur at 3100, 4300, and 5500 THz. When the virus diameter is 100 nm, the three lowest frequencies become 1600, 2300, and 2900 THz. The latter frequencies correspond to about half the former, indicating the inverse relation between the resonance frequency and virus size. Although the virus model is multilayered with different permittivity values, the obtained resonances are similar to the dielectric spheres model in [53]. It can also be seen that the resonance response is relatively wide, with a percentage bandwidth between 20 to 40%.

Virus sizes differ from case to case. However, as the resonance response is not sharp, size differences can be accommodated by the reasonably wide response. On the other hand, a relatively wideband UV light source is needed, and preferably more than one band will be more effective. Also, the effect of EM wave polarization on the power loss and deposition in the virus body is investigated. To that end, EM waves across the 100-600 THz with linear and circular polarization were used to interact with the virus body.

The power loss in the virus body results from the different dielectric properties of the virus's biological materials. It helps to determine the level of the EM radiation required to inflict damage or deactivate the virus envelope layer.

Therefore, the power loss monitor was assigned across the entire band with a step of 100 THz. The power loss monitor reading provides the power loss density value $\left(w/cm^3\right)$ when the EM waves interact with the virus body. The result generally shows that the power loss density across the entire band at higher frequencies is bigger than at lower frequencies when both linear and circular polarized EM waves are used. However, the maximum power loss occurs at the resonant frequencies, and the location of the maximum loss is always in the enveloping layer. The power loss density is presented at the resonant frequencies in Figs. 6-9 taking a cross-section in the YZ-plane laying at x = 0.

Fig. 7.

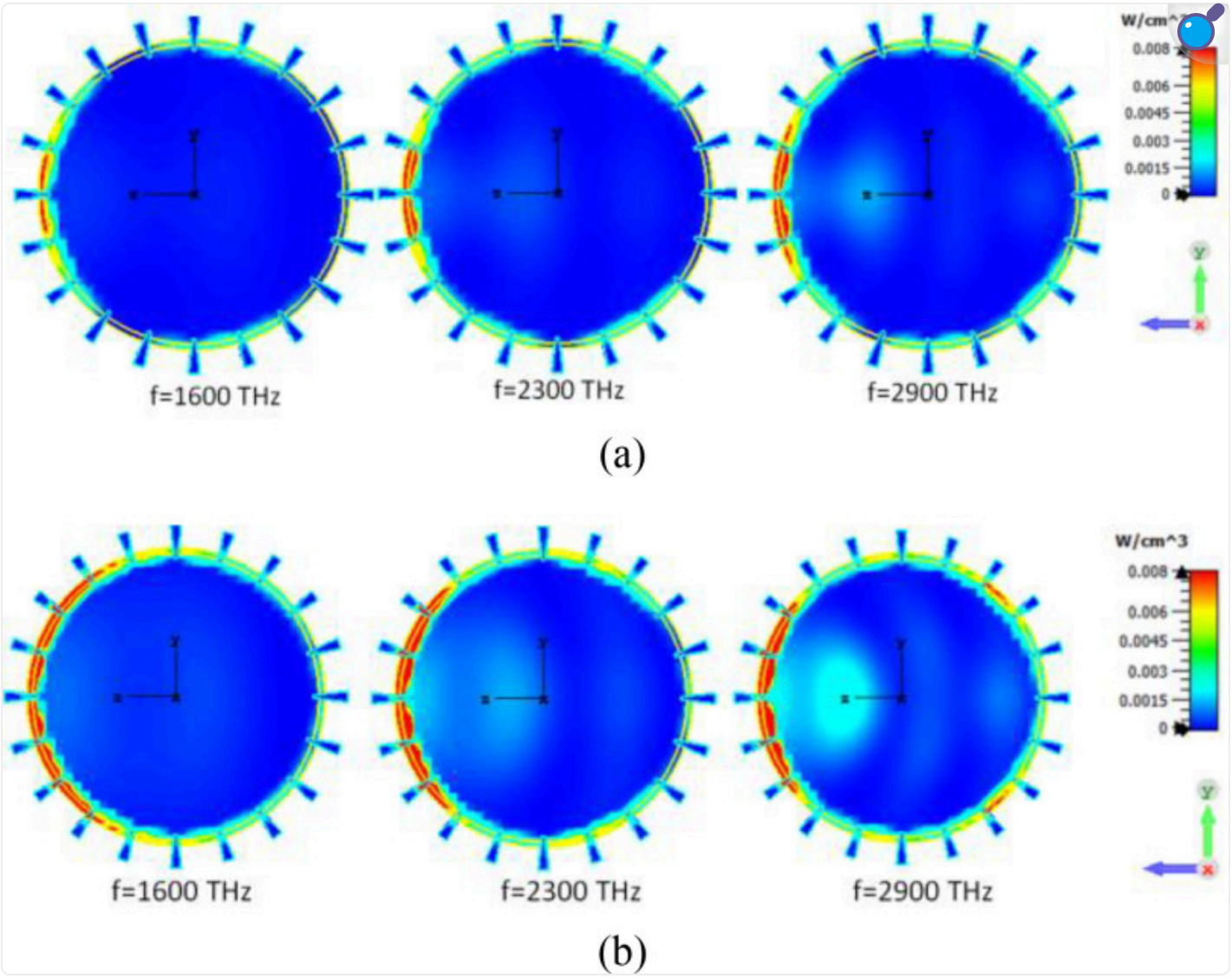

Open in a new tab

The power loss in the envelope for virus RNA diameter 100 nm (a) linear polarization EM wave, (b) circular polarization EM wave.

Fig. 8.

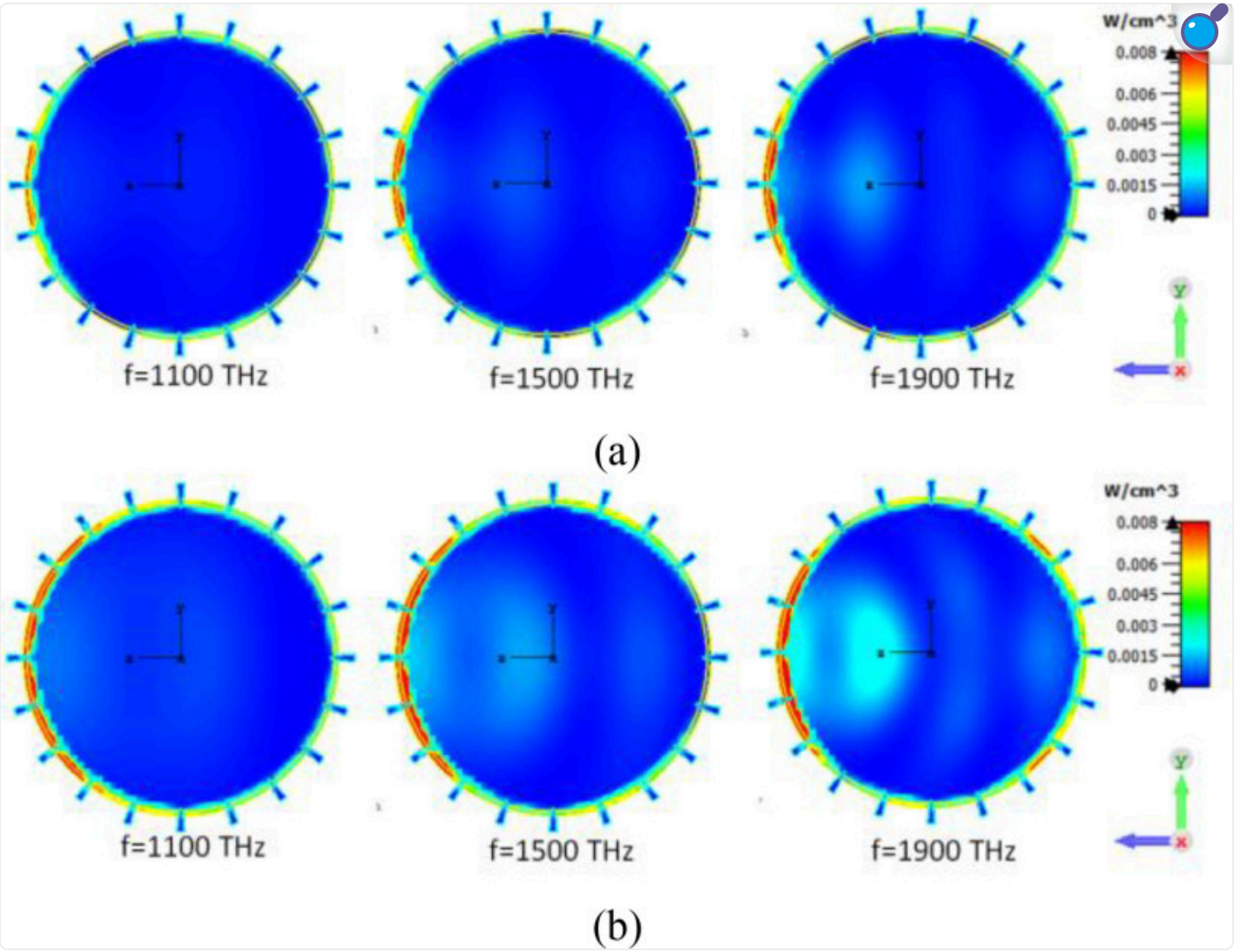

Open in a new tab

The power loss in the envelope for virus RNA diameter 150 nm (a) linear polarization EM wave, (b) circular polarization EM wave.

Fig. 6.

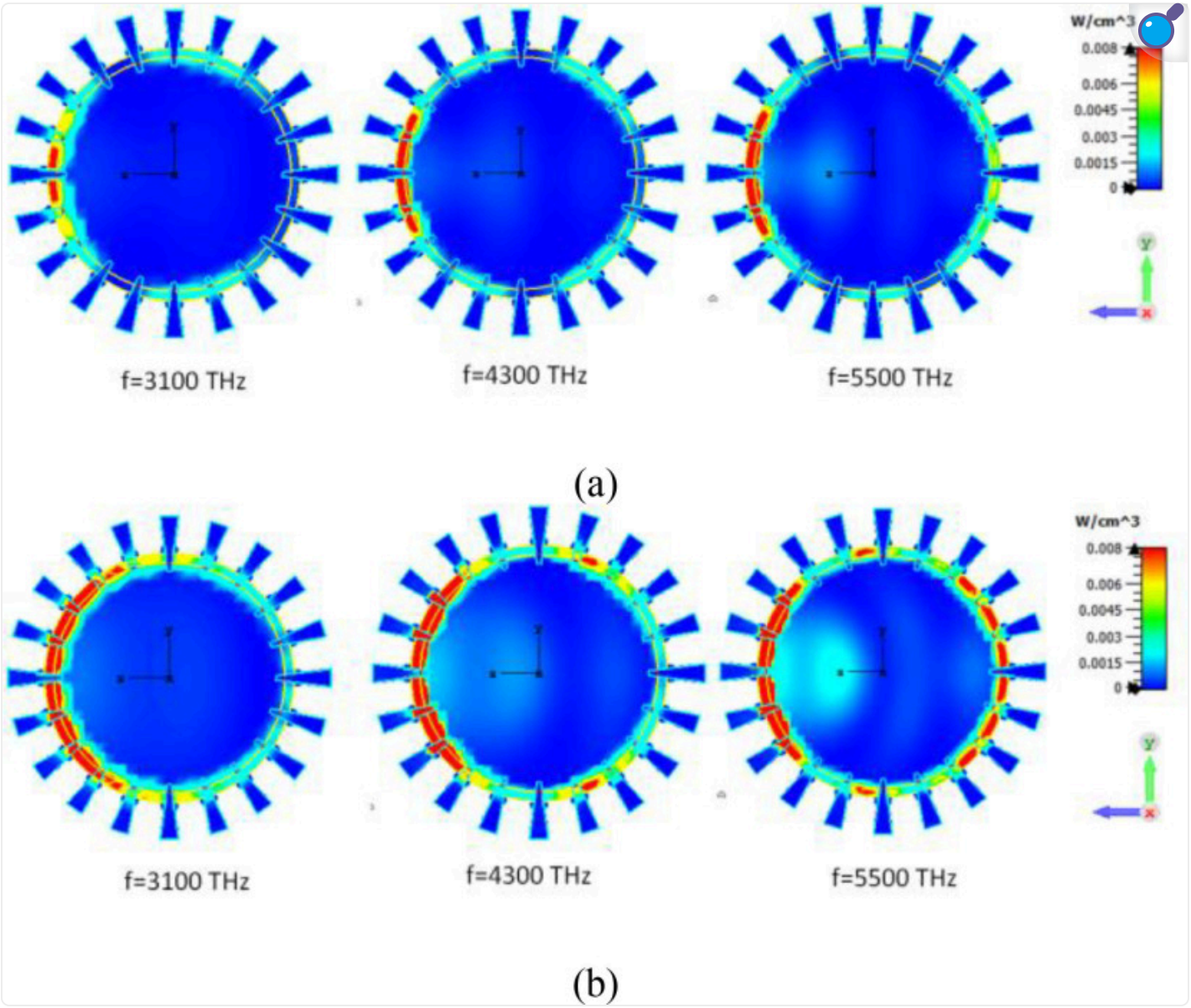

Open in a new tab

The power loss in the envelope for virus RNA diameter 50 nm (a) linear polarization EM wave, (b) circular polarization EM wave.

Fig. 9.

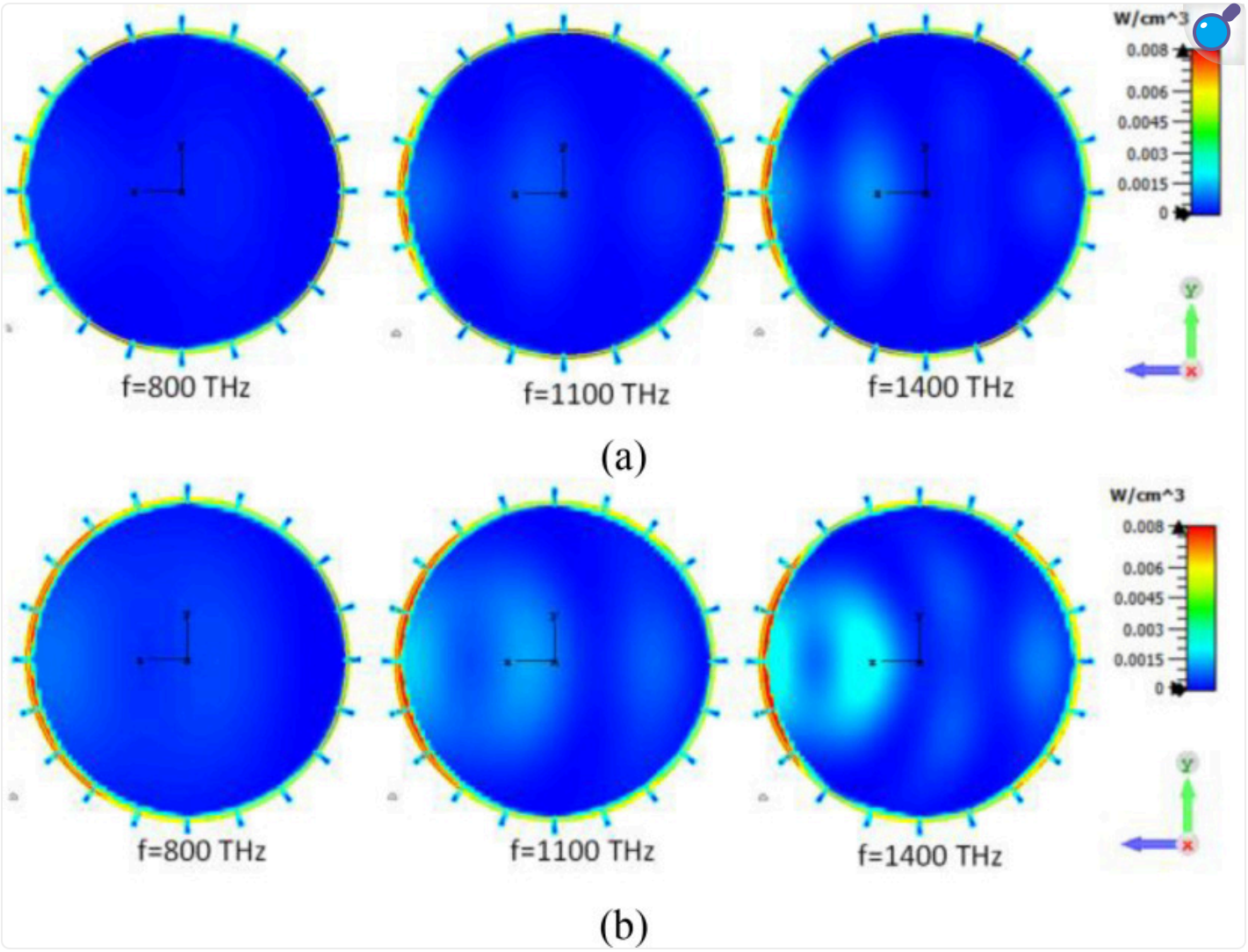

Open in a new tab

The power loss in the envelope for virus RNA diameter 200 nm (a) linear polarization EM wave, (b) circular polarization EM wave.

The simulation results show that the maximum power loss always appeared on the other side of the sphere (away from the irradiating source) using linear and circular polarizations across all the resonant frequencies. The minimum power loss occurred on the side of the sphere facing the wave source for all the virus sizes. Larger power densities were noticed on the enveloping layer compared to other parts of the virus model. For small viruses of 50 nm RNA diameter, the maximum power loss in the envelope occurs at 550 THz. The maximum losses in the envelope

layer for the virus of 100 and 150 nm RNA diameter occur at (5700 THz). The maximum power for virus RNA diameter of 200 nm occurs at 5000 and 5300 THz. Regarding the effect of the polarization on the virus body, the results show that stronger interaction occurs with the virus body when circular polarization is used. Table II summarizes the details of the maximum power loss in the envelope layer for all virus sizes for both linear and circular polarization.

TABLE II. The Maximum Power Loss Density in the Enveloping Layer for Em Waves Applied with Linear and Circular Polarazation.

Virus RNA diameter	**Resonant frequency (THz)**	$P_d(\frac{w}{cm^2})\times 10^2$**(Linear, Circular)**
50 nm	3100/4300/5500	(12.5)/ (37.8)/ (4.712)
100 nm	1600/2300/2900 3200/3500/3800 4100/4400/4600 4900/5200/5500/ 5700	(1.1, 2.5)/ (24.6)/ (2.81.3) (51.2)/ (3.67.8)/ (51.1) (71.6)/ (9.62.3)/ (10,2.4) (10,2.5)/ (10,2.4)/ (10,2.4)/ (1.33.2)
150 nm	1100/1500/1900 2200/2600/2900 3100/3300/3700 4100/4400/4600 4800/5300/5700/ 5900	(1.22.7)/ (24.6)/ (37) (51.1,)/ (5.61.2)/ (5.61.2) (5, 1.1)/ (5.61.2)/ (5.61.2) (92.1)/ (1.433)/ (1.12.5) (1.43.3)/ (1.63.6)/ (24.9)/ (24.7)
200 nm	800/1100/1400 1700/2200/2500 2800/3100/3700 4000/4300/4600 5000/5300/5900	(1.12.4)/ (2.24.7)/ (3.67.5) (510)/ (61.3)/ (5.61.2) (5.31.1)/ (1.22.3)/ (2.24.3) (1.62.8)/ (3.25.5)/ (34.9) (4.37.9)/ (36.3)/ (3.78.3)

Open in a new tab

It can be observed from the results shown in Figs. 6-9 that higher power density is placed in the envelope for various sizes of the virus using linear and circular polarizations. Thus, the heating

effect will be concentrated in the envelope of the virus, which is the most vulnerable part of the virus. This can be seen as a favourable property of UV irradiation since a lower power level is needed to inactivate the virus than when the incident power is evenly distributed across the whole parts of the virus.

B. The Total Power

The power required for destroying or inactivating the virus may be estimated from the required temperature rise of the envelope to inflect the damage, but such a result has not been established in the literature. However, many published experimental results relate the inactivation rate to the incident power density ($mW/cm2$) and irradiation time. The inactivation rate compares the number of active viruses before irradiation (Nb) and after irradiation (Na). An algorithmic ratio defines it as:

$$Inactivation = log10\frac{Nb}{Na} \ldots\ldots\ldots \quad (5)$$

Thus, an inactivation value of 3 means that only 0.1% of the eradicated viruses remain. The power density and irradiation time in seconds can be combined to give energy density expressed in ($mJ/cm2$). Various energy density rates, power density levels, and exposure times have been reported. An average UV dose of 1.3 $mJ/cm2$ was required to yield a 1-log inactivation of SARS-CoV-2 using the LP UV lamp (254 nm) [54]. This is similar to other results of 1.2 to 5.0 mJ/cm^2 for 1-log inactivation published in [55]–[57]. In recent experimental results, a wavelength of 278 nm at an energy density dose of 2.07 $mJ/cm2$ was found to result in an inactivation of 2-Log (1% of the irradiated viruses remained unaffected) [58]. The same Log reduction was achieved by a dose of 10 $mJ/cm2$ at 265 nm [59] and by a dose of 2 $mJ/cm2$, and 4 $mJ/cm2$ using 270 nm and 282 nm respectively [54].The wide range of power densities, irradiation time, and energy density published by researchers can be attributed to the various virus sizes, used wavelengths, and experimental environments. The above results confirm the obtained results of this work regarding the finding that power deposition shows resonance at specific frequencies.

Moreover, they show that treatment by UV irradiation is a feasible modality. When the power needed to inactivate one virus is determined, then one can find the total power required to destroy viruses to the required inactivation level defined by (4), in one oral activity such as a cough or cough sneeze using (3). Although one cough may contain virus copies of different sizes mixed,

depending on the size of the droplets. However, in this work, the calculation is made by considering that the cough has the same size droplets, which means all the viruses have the same size. Figs. 10-11 show the results, and the total deposited power increases with the number of copies. Also, more power is required when the size of the virus increases. Moreover, the required power to destroy the envelop layer increases with the virus size. Therefore, the total deposited power is calculated for the two scenarios: the average number and the maximum number of viruses available in an infected area.

Fig. 10.

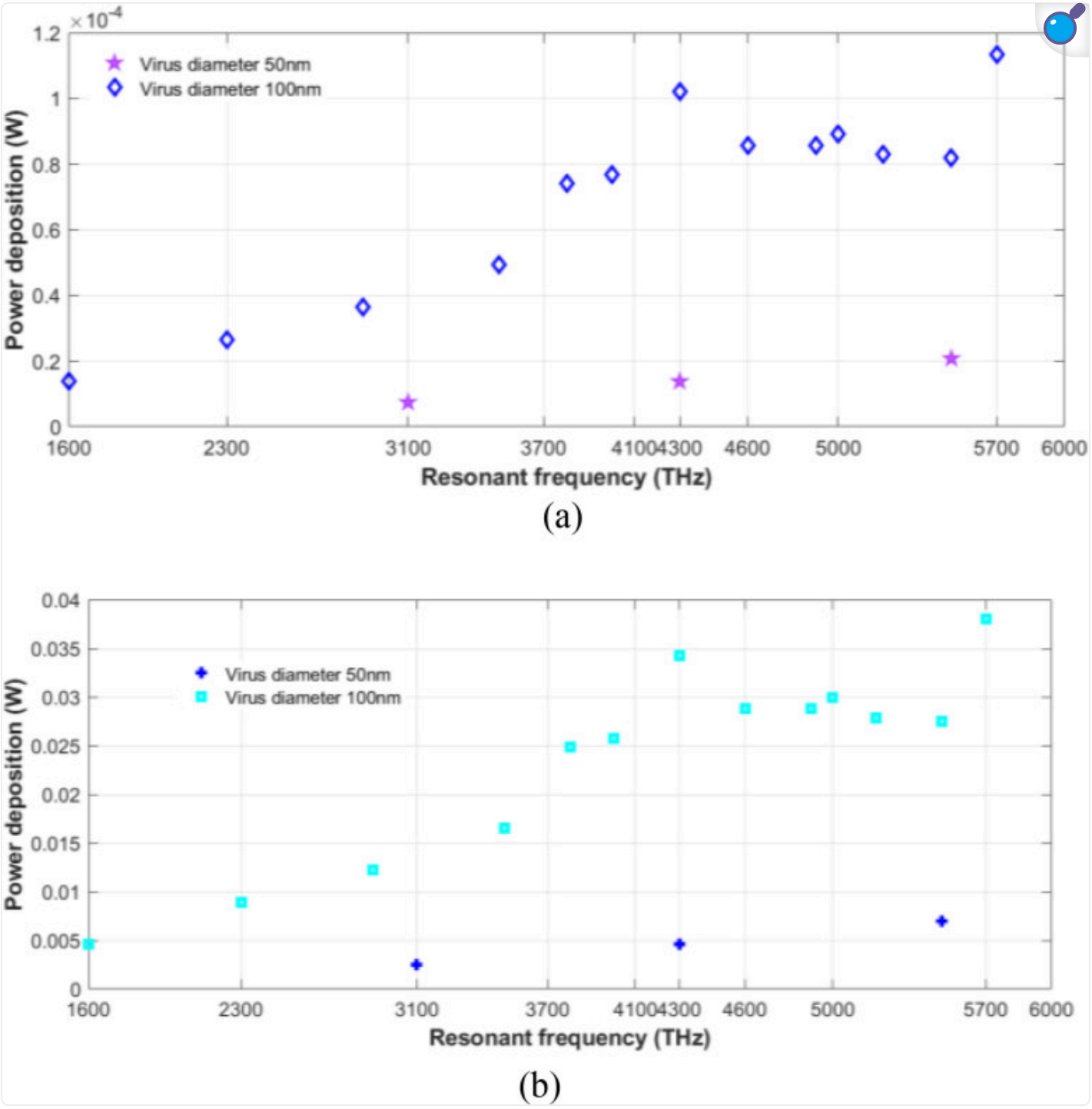

Open in a new tab

The total deposited power in one cough droplet containing 50 and 100 nm virus RNA diameter at resonant frequencies (a) the Average number of virus copies (b) the maximum number of virus copies.

Fig. 11.

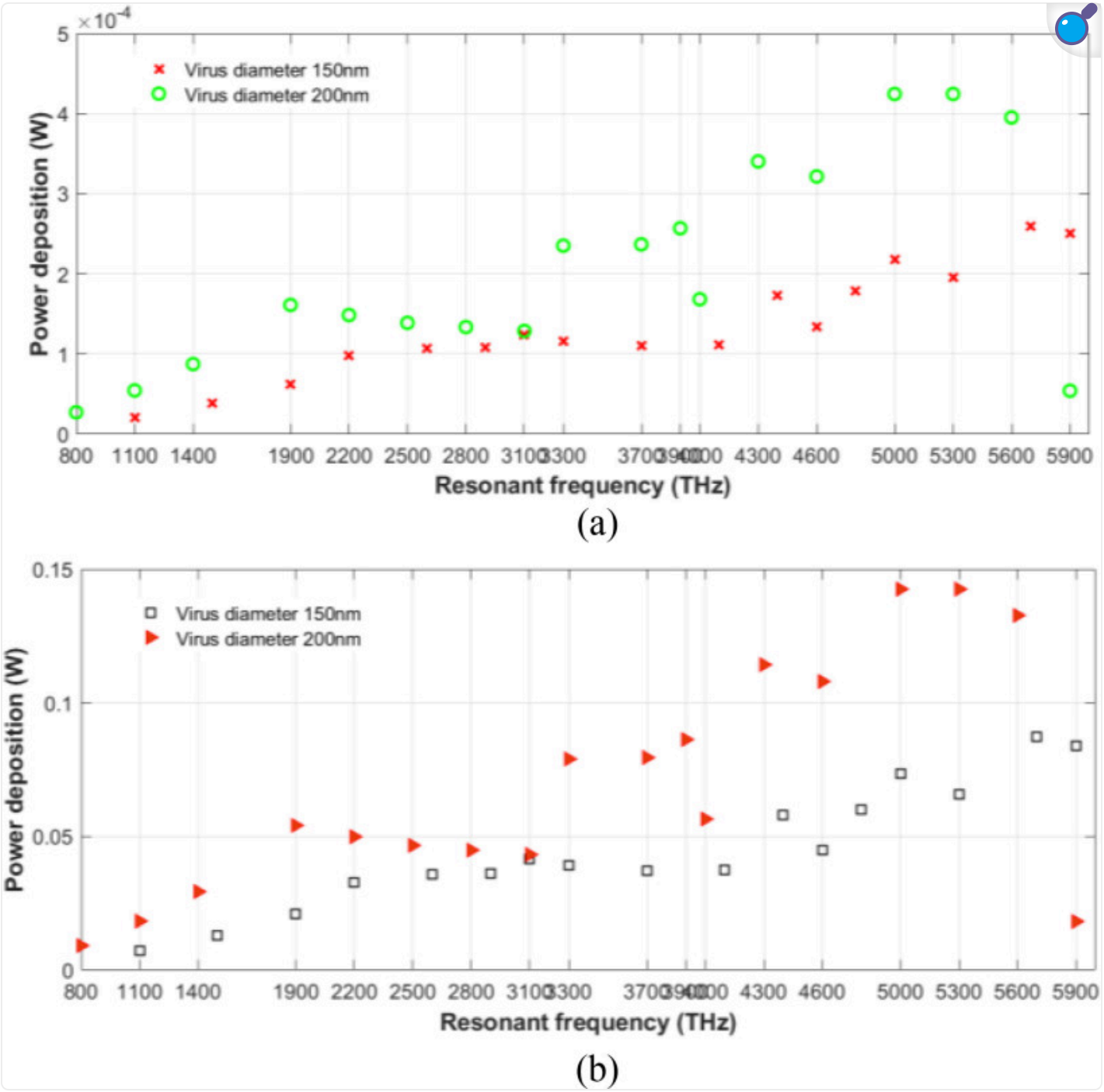

Open in a new tab

The total deposited power in one cough droplet containing 150 and 200 nm virus RNA diameter at resonant frequencies (a) the Average number of virus copies (b) the maximum number of virus copies.

IV. Conclusion

A simulation study has been conducted to investigate effects of electromagnetic resonance absorption on COVID-19 virus. Realistic virus body structures with different sizes were modeled using their estimated dielectric properties across the 100-6000 THz frequency band. The results confirm an inverse relation between the resonance frequency and virus size, whereas the relation is direct between the virus size and its power absorption. It is also concluded that the high-power density is always deposited in the virus envelope irrespective of the virus size and used polarization. Thus, the heating effect is concentrated in the virus envelope, which is the most vulnerable part of the virus. This is a favourable property of UV irradiation since a lower power level is needed to inactivate the virus compared with the case when the incident power is evenly distributed across all parts of the virus.

In addition, the total power required to destroy and damage the virus in an oral activity (i.e., cough) can be estimated if the power needed to inactivate one virus is established. The results show that the total power increases when the virus copies in the activity increase. As a result, larger number and size of viruses require higher power to destroy their envelope layers and terminate them.

This study furnishes the theoretical evidence of the recently published observations regarding the use of UV light for virus disinfection. This work presents the theoretical principle that explains why the recently published observations on the relation between required power densities to inactivate the virus and the used wavelengths. Furthermore, this study explains the effective use of irradiation by a proper dose of UV-C band to eradicate the virus.

Contributor Information

Khalil H. Sayidmarie, Email: kh.sayidmarie@gmail.com.

Beadaa Mohammed, Email: b.mohammed@uq.edu.au.

Asmaa J. Mohammed, Email: yazinshahd@gmail.com.

Amin Abbosh, Email: a.abbosh@uq.edu.au.

References

[1]. Wiersinga W. J., Rhodes A., Cheng A. C., Peacock S. J., and Prescott H. C., "Pathophysiology, transmission, diagnosis, and treatment of coronavirus disease 2019 (COVID-19): A review," Jama, vol. 324, no. 8, pp. 782–793, 2020. [DOI] [PubMed] [Google Scholar]

[2]. Flythe J. E. et al. , "Characteristics and outcomes of individuals with pre-existing kidney disease and COVID-19 admitted to intensive care units in the United States," Amer. J. Kidney Dis., vol. 77, no. 2, pp. 190–203, 2021. [DOI] [PMC free article] [PubMed] [Google Scholar]

[3]. Di Gennaro F. et al. , "Coronavirus diseases (COVID-19) current status and future perspectives: A narrative review," Int. J. Environ. Res. Public Health, vol. 17, no. 8, pp. 2690–2701, 2020. [DOI] [PMC free article] [PubMed] [Google Scholar]

[4]. Zhang L. et al. , "Crystal structure of SARS-CoV-2 main protease provides a basis for design of improved α-ketoamide inhibitors," Science, vol. 368, no. 6489, pp. 409–412, 2020. [DOI] [PMC free article] [PubMed] [Google Scholar]

[5]. Chen N. et al. , "Epidemiological and clinical characteristics of 99 cases of 2019 novel coronavirus pneumonia in Wuhan, China: A descriptive study," Lancet, vol. 395, no. 10223, pp. 507–513, 2020. [DOI] [PMC free article] [PubMed] [Google Scholar]

[6]. World Health Organization, "Novel coronavirus (2019-nCoV): Strategic preparedness and response plan," Feb. 2020. [Online]. Available: https://www.who.int/docs/default-source/coronaviruse/srp-04022020

[7]. Jee Y., "WHO international health regulations emergency committee for the COVID-19 outbreak," Epidemiol. Health, vol. 42, 2020,. Art. no. e2020013. [DOI] [PMC free article] [PubMed] [Google Scholar]

[8]. Wu S. C., "Progress and concept for COVID-19 vaccine development," Biotechnol. J., vol. 15, no. 6, Jun. 2020,. Art. no. 2000147. [DOI] [PMC free article] [PubMed] [Google Scholar]

[9]. Dong Y. et al. , “Epidemiology of COVID-19 among children in China,” Pediatrics, vol. 145, no. 6, pp. 1–10, 2020. [DOI] [PubMed] [Google Scholar]

[10]. World Health Organization, “Advice for the public: Coronavirus disease (COVID-19),” Oct. 2021. [Online]. Available: https://www.who.int/emergencies/diseases/novel-coronavirus-2019/advice-for-public

[11]. World Health Organization, “Infection prevention and control of epidemic-and pandemic-prone acute respiratory diseases in health care: WHO interim guidelines,” World Health Org., Geneva, Switzerland, Reference Number WHO/CDS/EPR/2007.6, 2007.

[12]. Wimalawansa S. J., “Global epidemic of coronavirus—COVID-19: What can we do to minimize risks,” Eur. J. Biomed., vol. 7, no. 3, pp. 432–438, 2020. [Google Scholar]

[13]. Cascella M., Rajnik M., Aleem A., Dulebohn S., and Di Napoli R., “Features, evaluation, and treatment of coronavirus (COVID-19),” StatPearls, Treasure Island, FL, USA: StatPearls Publishing, 2022. [PubMed]

[14]. Dogra A., Goyal B., and Sharma A. M., “Corona virus: A novel outbreak,” Biomed. Pharmacol. J., vol. 13, no. 1, pp. 5–10, 2020. [Google Scholar]

[15]. Gerchman Y., Mamane H., Friedman N., and Mandelboim M., “UV-LED disinfection of coronavirus: Wavelength effect,” J. Photochemistry Photobiol. B: Biol., vol. 212, pp. 112044–112050, 2020. [DOI] [PMC free article] [PubMed] [Google Scholar]

[16]. Carleton T., Cornetet J., Huybers P., Meng K. C., and Proctor J., “Global evidence for ultraviolet radiation decreasing COVID-19 growth rates,” Proc. Nat. Acad. Sci., vol. 118, no. 1, 2021, Art. no. e2012370118. [DOI] [PMC free article] [PubMed] [Google Scholar]

[17]. Verma S. S., “Killing coronavirus with ultraviolet light,” Indian Practitioner, vol. 73, no. 10, pp. 7–9, 2020. [Google Scholar]

[18]. Kumar A., Sagdeo A., and Sagdeo P. R., “Possibility of using ultraviolet radiation for disinfecting the novel COVID-19,” Photodiagnosis Photodynamic Ther., vol. 34, pp. 102234–102235, 2021. [DOI] [PMC free article] [PubMed] [Google Scholar]

[19]. Valagiannopoulos C. and Sihvola A., “Maximal interaction of electromagnetic radiation with corona virions,” Phys. Rev. B, vol. 103, no. 1, pp. 14114–14124, 2021. [Google Scholar]

[20]. Cordero-Samortin A., Dela Cruz J. C., Garcia R., and Mabunga Z., “The effect of various ultra high frequency radiation on the evolution of the staphylococcus aureus,” in Proc. IEEE 12th Int. Conf. Humanoid, Nanotechnol., Inf. Technol., Commun. Control, Environ., Manage., 2020, pp. 1–6. [Google Scholar]

[21]. CST Microwave Studio, CST Studio Suite, Computer Simulation Technology AG., 2008.

[22]. Kirtipal N., Bharadwaj S., and Kang S. G., “From SARS to SARS-CoV-2, insights on structure, pathogenicity and immunity aspects of pandemic human coronaviruses,” Infection, Genet. Evol., vol. 85, pp. 104502–104517, 2020. [DOI] [PMC free article] [PubMed] [Google Scholar]

[23]. DCD Organization, “Centeres for disease control and presventation,” Digital Lirary Coronavirus, 2020. [Online]. Available: https://www.cdc.gov/media/subtopic/images.htm

[24]. Heßling M., Hönes K., Vatter P., and Lingenfelder C., “Ultraviolet irradiation doses for coronavirus inactivation–review and analysis of coronavirus photoinactivation studies,” GMS Hyg. Infection Control, vol. 15, 2020, Art. no. Doc08, doi: 10.3205/dgkh000343. [DOI] [PMC free article] [PubMed] [Google Scholar]

[25]. Zhu N. et al. , “A novel coronavirus from patients with pneumonia in China,” New England J. Med., vol. 382, pp. 727–733, 2020, doi: 10.1056/NEJMoa2001017, PMID: 31978945, 2019. [DOI] [PMC free article] [PubMed] [Google Scholar]

[26]. A. Eckert, MSM, D. Higgins, and MAMSvd. “Public health image library,” Centers for Disease Control and Prevention, [Online]. Available: https://phil.cdc.gov/ImageidSearch.aspx?imgid=23311

[27]. Petrov D., “Photopolarimetrical properties of coronavirus model particles: Spike proteins number influence,” J. Quantitative Spectrosc. Radiative Transfer, vol. 248, pp. 107005–107014, 2020. [DOI] [PMC free article] [PubMed] [Google Scholar]

[28]. Shang J. et al. , “Cell entry mechanisms of SARS-CoV-2,” Proc. Nat. Acad. Sci., vol. 117, no. 21, pp. 11727–11734, 2020. [DOI] [PMC free article] [PubMed] [Google Scholar]

[29]. Noman A. et al. , “Spike glycoproteins: Their significance for corona viruses and receptor binding activities for pathogenesis and viral survival,” Microbial Pathogenesis, vol. 151, pp. 104719–104728, 2021. [DOI] [PMC free article] [PubMed] [Google Scholar]

[30]. Callaway E., “Making sense of coronavirus mutations,” Nature, vol. 585, no. 7824, pp. 174–177, 2020. [DOI] [PubMed] [Google Scholar]

[31]. Pachetti M. et al. , “Emerging SARS-CoV-2 mutation hot spots include a novel RNA-dependent-RNA polymerase variant,” J. Transl. Med., vol. 18, no. 1, pp. 1–9, 2020. [DOI] [PMC free article] [PubMed] [Google Scholar]

[32]. Jungreis I., Sealfon R., and Kellis M., “SARS-CoV-2 gene content and COVID-19 mutation impact by comparing 44 *Sarbecovirus* genomes,” Nature Commun., vol. 12, no. 1, pp. 1–20, 2021. [DOI] [PMC free article] [PubMed] [Google Scholar]

[33]. Abdelrahman Z., Li M., and Wang X., “Comparative review of SARS-CoV-2, SARS-CoV, MERS-CoV, and influenza a respiratory virus,” Front. Immunol., vol. 11, 2020, Art. no. 2309. [DOI] [PMC free article] [PubMed] [Google Scholar]

[34]. V'kovski P., Kratzel A., Steiner S., Stalder H., and Thiel V., “Coronavirus biology and replication: Implications for SARS-CoV-2,” Nature Rev. Microbiol., vol. 19, no. 3, pp. 155–170, 2021. [DOI] [PMC free article] [PubMed] [Google Scholar]

[35]. Stevens L. J. et al. , “Mutations in the SARS-CoV-2 RNA dependent RNA polymerase confer resistance to remdesivir by distinct mechanisms,” Sci. Transl. Med., vol. eabo0718, pp. 1–22, 2022. [DOI] [PMC free article] [PubMed] [Google Scholar]

[36]. Mata-Portuguez V. H., Pérez L. S., and Acosta-Gío E., “Sterilization of heat-resistant instruments with infrared radiation,” Infection Control Hosp. Epidemiol., vol. 23, no. 7, pp. 393–396, 2020. [DOI] [PubMed] [Google Scholar]

[37]. Hamanaka D., Uchino T., Furuse N., Han W., and Tanaka S. I., “Effect of the wavelength of infrared heaters on the inactivation of bacterial spores at various water activities,” Int. J. Food Microbiol., vol. 108, no. 2, pp. 281–285, 2006. [DOI] [PubMed] [Google Scholar]

[38]. Banerjee S., Raghunathan S., Banerjee S., and Bandyopadhyay B., “Portable sterilizer with microbe content detection device,” Bull. Nat. Res. Centre, vol. 45, no. 1, pp. 1–5, 2021. [DOI] [PMC free article] [PubMed] [Google Scholar]

[39]. Lu Z. Y., Ding H., Sun W. Q., and Andshi P. P., “The study on experiment and mechanism of sterilization with electromagnetic wave,” J. Electromagn. Waves Appl., vol. 21, no. 6, pp. 729–735, 2007. [Google Scholar]

[40]. Hamanaka D., Uchino T., Furuse N., Han W., and Tanaka S. I., “Effect of the wavelength of infrared heaters on the inactivation of bacterial spores at various water activities,” Int. J. Food Microbiol., vol. 108, no. 2, pp. 281–285, 2006. [DOI] [PubMed] [Google Scholar]

[41]. Cuervo A., Dans P. D., Carrascosa J. L., Orozco M., Gomila G., and Fumagalli L., “Direct measurement of the dielectric polarization properties of DNA,” Proc. Nat. Acad. Sci., vol. 111, no. 35, pp. E3624–E3630, 2014. [DOI] [PMC free article] [PubMed] [Google Scholar]

[42]. Hasgall P. A. et al. , “IT'IS database for thermal and electromagnetic parameters of biological tissues,” Version 4.1, Feb. 22, 2022, doi: 10.13099/VIP21000-04-1. [DOI]

[43]. Tadepalli S. P., “Novel remedial approaches against virulent corona viruses,” Int. J. Infect. Dis. Res., vol. 1, no. 1, pp. 1–15, 2020. [Google Scholar]

[44]. Gun L. and Ning D., “Equivalent permittivity based on debye model of blood and its SAR,” IJSTS, vol. 5, no. 3, pp. 37–40, 2017. [Google Scholar]

[45]. Almog I. F., Bradley M. S., and Bulovic V., The Lorentz oscillator and Its Applications. Cambridge, MA, USA: Massachusetts Inst. Technol., 2011. [Google Scholar]

[46]. Mittal R., Ni R., and Seo J. H., “The flow physics of COVID-19,” J. Fluid Mechanics, vol. 894, no. 2, pp. 1–14, 2020. [Google Scholar]

[47]. Bourouiba L., “Turbulent gas clouds and respiratory pathogen emissions: Potential implications for reducing transmission of COVID-19,” Jama, vol. 323, no. 18, pp. 1837–1838, 2020. [DOI] [PubMed] [Google Scholar]

[48]. Asadi S., Bouvier N., Wexler A. S., and Ristenpart W. D., “The coronavirus pandemic and aerosols: Does COVID-19 transmit via expiratory particles?,” Aerosol Sci. Technol., vol. 54, no. 6, pp. 635–638, 2020. [DOI] [PMC free article] [PubMed] [Google Scholar]

[49]. Chartier Y. and Pessoa-Silva C. L., Natural Ventilation for Infection Control in Health-Care Settings. Geneva, Switzerland: World Health Org., 2009. [PubMed] [Google Scholar]

[50]. Dhand R. and Li J., “Coughs and sneezes: Their role in transmission of respiratory viral infections, including SARS-CoV-2,” Amer. J. Respir. Crit. Care Med., vol. 202, no. 5, pp. ;651–659, 2020. [DOI] [PMC free article] [PubMed] [Google Scholar]

[51]. Morawska L. and Cao J., “Airborne transmission of SARS-CoV-2: The world should face the reality,” Environ. Int., vol. 139, pp. 105730–105733, 2020. [DOI] [PMC free article] [PubMed] [Google Scholar]

[52]. Wofel R. et al. , “Virological assessment of hospitalized patients with COVID-2019,” Nature, vol. 581, pp. 465–469, 2020. [DOI] [PubMed] [Google Scholar]

[53]. Tribelsky1 M. I., Geffrin J. M., Litman A., Eyraud C., and Moreno M. F., "Small dielectric spheres with high refractive index as new multifunctional elements for optical devices," Sci. Rep., vol. 5, pp. 12288–12295, 2015. [DOI] [PMC free article] [PubMed] [Google Scholar]

[54]. Ma B., Gundy P. M., Gerba C. P., Sobsey M. D., and Linden K. G., "UV inactivation of SARS-CoV-2 across the UVC spectrum: KrCl* excimer, mercury-vapor, and light-emitting-diode (LED) sources," Appl. Environ. Microbiol., vol. 87, no. 22, Nov. 2021, Art. no. e01532. [DOI] [PMC free article] [PubMed] [Google Scholar]

[55]. Biasin M. et al. , "UV-C irradiation is highly effective in inactivating SARS-CoV-2 replication," Sci. Rep., vol. 11, pp. 6260–6267, 2021, doi: 10.1038/s41598-021-85425-w. [DOI] [PMC free article] [PubMed] [Google Scholar]

[56]. Patterson E. I. et al. , "Methods of inactivation of SARS-CoV-2 for downstream biological assays," J. Infect. Dis., vol. 222, pp. 1462–1467, 2020, doi: 10.1093/infdis/jiaa507. [DOI] [PMC free article] [PubMed] [Google Scholar]

[57]. Storm N. et al. , "Rapid and complete inactivation of SARS-CoV-2 by ultraviolet-C irradiation," Sci. Rep., vol. 10, pp. 22421–22425, 2020, doi: 10.1038/s41598-020-79600-8. [DOI] [PMC free article] [PubMed] [Google Scholar]

[58]. Biasin M. et al. , "UV and violet light can neutralize SARS-CoV-2 infectivity," J. Photochemistry Photobiol., vol. 10, 2022, Art. no. 100107, [Online]. Available: https://www.sciencedirect.com/science/article/pii/S2666469021000920 [DOI] [PMC free article] [PubMed] [Google Scholar]

[59]. Shimoda H., Matsuda J., Iwasaki T., and Hayasaka D., "Efficacy of 265-nm ultraviolet light in inactivating infectious SARS-CoV-2," J. Photochemistry Photobiol., vol. 7, 2021, Art. no. 100050, doi: 10.1016/j.jpap.2021.100050. [DOI] [PMC free article] [PubMed] [Google Scholar]
